Experimental investigation of the combined effects of a split-ring damper and an intentional mistuning pattern on a blisk forced response

Salvador Rodríguez-Blanco, Valdo Pagès, Nicolas Guérin, Laurent Blanc, Cécile Dumartineix, Claude Gibert, Fabrice Thouverez

EXPERIMENTAL INVESTIGATION OF THE COMBINED EFFECTS OF A SPLIT-RING DAMPER AND AN INTENTIONAL MISTUNING PATTERN ON A BLISK FORCED RESPONSE

Salvador Rodríguez-Blanco[1,*], Valdo Pagès[2], Nicolas Guérin[3], Laurent Blanc[4], Cécile Dumartineix[2], Claude Gibert[4], Fabrice Thouverez[4]

[1]Universidad Politécnica de Madrid, Madrid, Spain
[2]Safran Aircraft Engines, Moissy-Cramayel, France
[3]ONERA - The French Aerospace Lab, Châtillon, France
[4]École Centrale de Lyon - LTDS - UMR 5513, Ecully, France

ABSTRACT

Friction damping is one of the main mechanisms for dissipating vibration energy in turbomachinery. For assembled bladed disks, friction typically arises in the blade root – in the disk interface or, for shrouded blade configurations, in the interface between two consecutive shrouds. For integrally bladed disks, where no such interface naturally occurs, additional damping devices must be designed if energy is to be dissipated through friction. Split-ring dampers are such devices: they are located in a circumferential groove under the blisk platform, and pressed onto it by centrifugal loads. At low vibration levels and/or high rotating speeds, the split ring remains stuck to the disk, while at high levels, relative motion starts and dissipates vibrational energy.

Such devices are often designed to mainly target a given nodal diameter mode of vibration. Nevertheless, designing these dampers is a challenging task. Indeed, their behavior depends on the design of the ring (dimensions, material and interface properties, etc.) and on the location of implementation; many different phenomena are involved such as centrifugal and thermal loading, mistuning,etc. Realistic contact modeling and simulation are also difficult because the dynamical behavior is non-linear due to the friction interfaces.

In this work, the effect of a split ring damper is investigated experimentally on an industrial compressor blisk in a vacuum chamber. A traveling wave excitation with a prescribed nodal diameter index is produced using piezoelectric actuators. Blade vibrations are monitored through strain gauges. Forced responses are measured, first on a tuned configuration activating the split ring damping effect on the targeted specific nodal diameter. Then an intentional mistuning pattern is implemented, so that the split ring target nodal diameter appears in different modes of the new configuration. The experiments show that resonance peaks are damped for different modes from that targeted at the tuned design stage.

Keywords: non-linear dynamics, bladed disk, split-ring damper, intentional mistuning, travelling wave response

NOMENCLATURE

AMM	Asymptotic mistuning model
BAE	Best achievable eigenvector
EO	Engine order
FRF	Frequency response function
ND	Nodal diameter
ROM	Reduced order model
TW	Travelling wave

1. INTRODUCTION

Integrally bladed disks - "blisks" - are important structural components in the turbomachinery industry. Due to their monoblock design, they afford valuable gains in mass compared to assembled bladed disks. Nevertheless, they endure severe mechanical conditions due to centrifugal stress and vibrational loading. This last point is all the more critical as only material and fluid damping can mitigate vibration amplitudes: indeed, due to the lack of contact interfaces, friction damping cannot occur between the blades and the disk as it can on assembled designs.

This is why additional damping devices are added, among them viscoelatic materials, underplatform friction

*Corresponding author: salvador.rodriguez@upm.es

dampers [1] [2], and often split-ring dampers [3]. The principle of action of split-ring dampers is that they are pressed by centrifugal loads onto the circumferential groove in which they are located, under the disk platform (see Fig. 1 and Fig. 2). At low vibration levels and/or high rotating speed, the split ring remains stuck to the disk, while at high levels, relative motion grows and the friction starts to dissipate vibrational energy. Such friction ring dampers are also used on other rotating parts, such as labyrinth seals [4], gears [5], or flywheels [6].

Another strategy to mitigate vibrational amplitude on blisks is the use of intentional mistuning: it has been proven that the well-chosen pattern and "level" of intentional mistuning (compared to natural mistuning) have a beneficial influence on vibrational fatigue and on the risk of instability, mainly by reducing the aerodynamic instability of the rotors [7], but also by reducing the amplification factor produced by natural mistuning [8].

The purpose here is to address the case where both intentional mistuning and split-ring strategies are implemented on the same blisk. The reason for this is that, on the one hand, the split-ring is typically designed to be efficient on a target nodal diameter of the tuned configuration, and on the other hand, intentional mistuning combines the different tuned blades. So it might be possible to activate the split-ring in the different mistuned modes which make a contribution to the targeted nodal diameter.

Some approaches do exist for the design and optimization of split-rings based on non-linear forced calculations [9] or modal analyses [10] [11] [12]. Certain methods to quantify intentional mistuning effects are also proposed [13] [14] [15]. But only a few papers present experiments [3] to validate split-ring designs, and even fewer offer a crossed study of split-rings and mistuning, even analytically [16]. Here, an experimental approach is adopted to show how resonance peaks are damped by the split-ring at different modes from the one targeted at the design stage, and to compare an intentionally mistuned design [17] forced response with a tuned design. This study is part of the European project ARIAS [18] aimed at developing new analysis methods, new measurement techniques and new technologies to mitigate harmful vibrations in complex aeromechanical behaviors that have not been previously investigated.

In the second section of this paper, the experimental set-up is presented: operating under vacuum to remove air influence, and under rotation to fix centrifugal effects. The blisk will be excited by traveling wave excitation with a given nodal diameter, and vibration levels will be obtained with strain gauges through a telemetry device (or by laser vibrometry at rest for calibration purposes). In section three, an intentional mistuning pattern is chosen based on the AMM method [17]. In section four, the experimental results

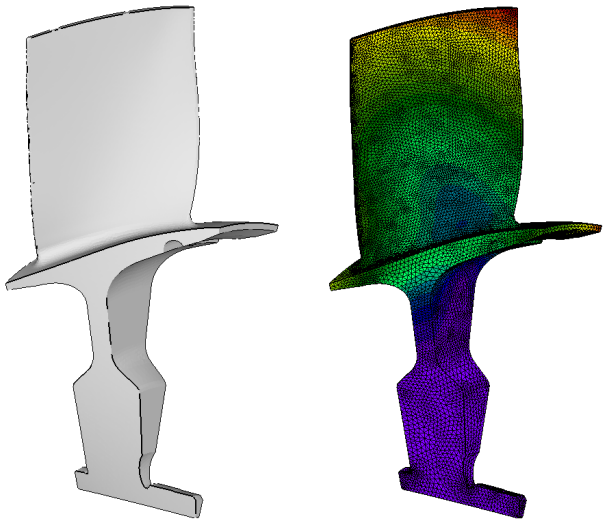

FIGURE 1: BLISK SECTOR: (LEFT) CAD MODEL (RIGHT) 2ND MODAL DISPLACEMENT AMPLITUDE FROM FEM.

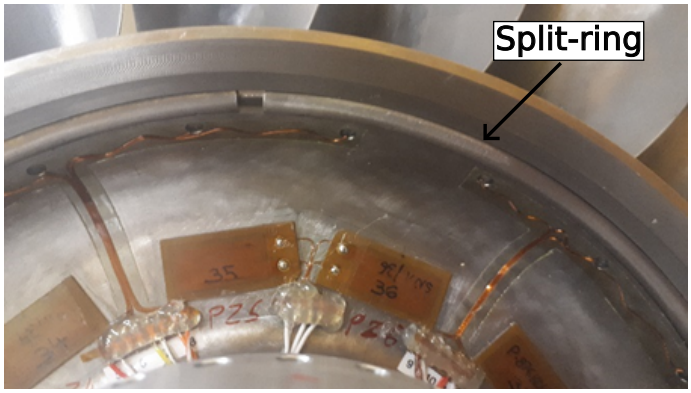

FIGURE 2: DETAILED VIEW OF THE BLISK WITH THE SPLIT-RING INSIDE ITS GROOVE AND PIEZOELECTRIC ACTUATORS.

are presented and discussed.

2. EXPERIMENTAL SETUP AND METHODS

2.1 The test structure

The purpose here is to study the coupled effect of intentional mistuning and a split-ring damper. The test structure is a 21-blade HP compressor blisk modified from a demonstrator designed in the FUTURE project [19]. A view of the geometry of an elementary sector is given in Fig. 1.

Concerning the split-ring, a new ring was manufactured, made of Inconel, with a diameter of 4 mm to be placed in a 6 mm groove. The split-ring was designed to be most effective at 5000 rpm for ND2 modes of the first, second and third modal families. The selected groove location with the split-ring inside is shown in Fig. 2. The mode mainly targeted for this study is the ND2 of the first bending family, whose modal shape is given in Fig. 1 (using a mesh of more than 19,000 elements per sector).

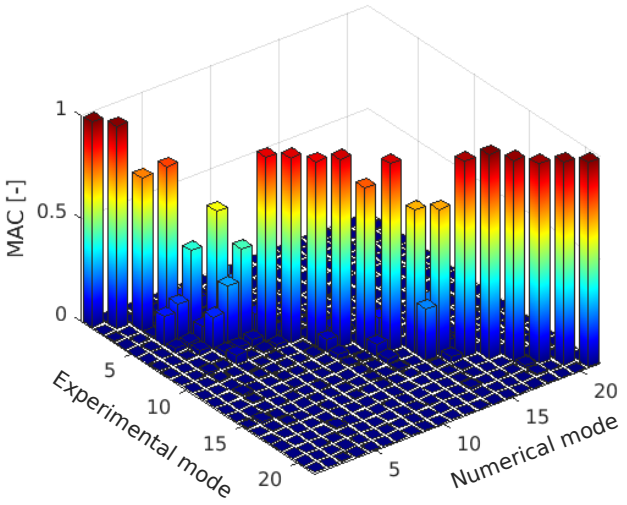

FIGURE 3: MAC BETWEEN NUMERICAL AND EXPERIMENTAL MODES AFTER UPDATING.

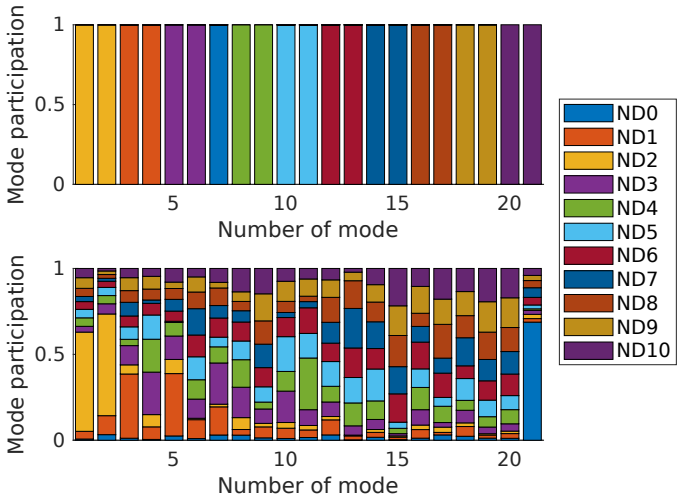

FIGURE 4: (TOP) TUNED NUMERICAL MODEL MODES ND CONTENT. (BOTTOM) MISTUNED NUMERICAL MODEL ND CONTENT AFTER BAE PROCEDURE (BASED ON EXPERIMENTAL MODES MEASUREMENT, BLISK SHAFT MOUNTED).

Concerning mistuning, a preliminary study was performed to minimize the effect of natural mistuning before implementing intentional mistuning: the principle was to evaluate the original mistuning pattern of the manufactured blisk and then to compensate for it.

Natural mistuning is potentially caused by manufacturing discrepancies, pressure sensors, etc. Its effect on modal parameters is included in the numerical model as a set of small concentrated masses located at homologous top corners of each blade. The assumption is that these masses can change tuned model eigenfrequencies and mode shapes sufficiently to fit the identified real blisk modes (with realistic mass values). Mass values identification is performed using the Best Achievable Eigenvector (BAE) method [20] for all measured modes simultaneously combined with a regularization technique, so that the numerical model fits the measurements in the best possible way in terms of the Modal Assurance Criterion (MAC) (Fig. 3). To do so, we developed a finite element model of the bladed disk and a computational reduced-order modeling technique based on the component mode substitution method. The ROM is obtained through the Craig-Bampton strategy. The full model's degrees of freedom are split into master DOFs and interior DOFs. Master DOFs are the 63 DOFs (Ux, Uy, Uz) of the 21 nodes where measurements have been performed (at blades corners). 100 interior modes are retained. The quality of the ROM is checked on the first three mode families, with an error on frequencies below 1%. BAE inputs are the natural frequencies and eigenvectors of the perfectly tuned numerical model, along with the actual modal parameters identified on the real blisk (Fig. 4).

To minimize natural mistuning, the opposites of the identified masses, with 0.01 g precision, are applied on the top corners of the blades (trailing edge, pressure side). The mass values implemented on the blisk must of course be positive, so the mass parameters are shifted to have zero as the minimal value. The masses were made by cutting a layer of 0.6 mm of brass into squares. The final distribution of the masses used with their location can be seen in (Fig. 5). These masses were glued using cyanocrylate on the tips of the blades.

The choice of intentional mistuning pattern is presented in Section 3.

2.2 General description of the test rig

The rig used to test the blisk presented above is devoted to studying the vibration of the rotating parts under vacuum conditions to remove aerodynamic effects (the main elements of the test rig are indicated in Fig. 6). It was initiated in the ADTurb II project to study damping effects in fir-tree attachments and underplatform dampers [21], and has been used in other projects, such as FUTURE and ARIAS, to study mistuning and split-rings.

Its spindle (Fig. 7) was adapted so that the blisk is connected by boltings in a sufficiently stiff manner in order to minimize dynamic coupling of the blisk with the shaft, at least in the targeted mode frequency range. The interface parts also support an electronic box with telemetry system, balancing masses and wiring. The shaft is hollow, among other things to convey the excitation power. It is driven by an electric motor at 0-5000 rpm, the rotational speed required to provide centrifugal effects. The tests are performed at ambient temperature.

2.3 Excitation

Excitation is supplied by a set of 12 encapsulated PZT piezoelectric patches (20x10x0.8 mm) working in d_{31} mode [22] and glued onto the blisk by means of an insulation device and epoxy resin (Fig. 2) and working in 31 mode (it

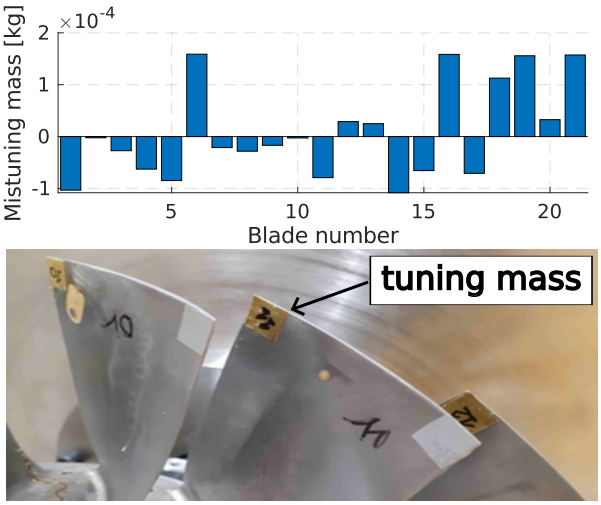

FIGURE 5: TOP: IDENTIFIED MISTUNING PATTERN ALONG THE BLADES. BOTTOM: IMPLEMENTATION OF THE TUNING MASSES.

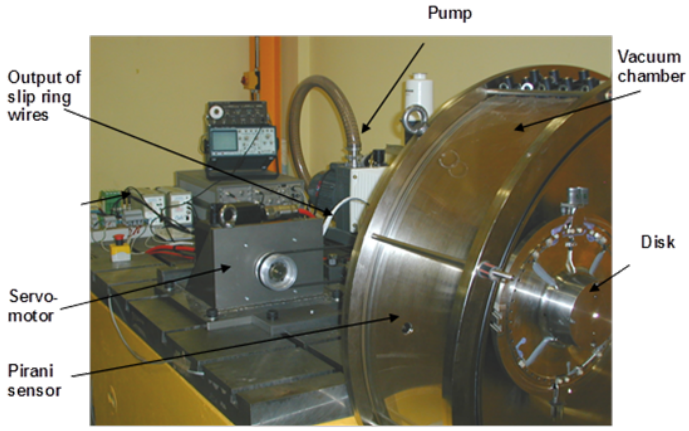

FIGURE 6: ADTURB II TEST RIG.

means that polarization occurs along the thickness, with a dilatation in the perpendicular directions). They are located circumferentially on the front face of the blisk hub. This configuration was chosen for several reasons: because a high level of vibration is numerically predicted to be reached by the models (sufficient to reach the fatigue limit on some target modes); because flat surfaces are available outside of the areas where the blisk is fixed to the shaft; because no mistuning is added onto the blades; and because the chosen areas are easy to work with in terms of gluing and wiring (to ensure better resistance to centrifugal forces and to minimize magnetic interference with the strain gauges).

Piezoelectric excitators can be activated independently of each other: depending on the law implemented in the control system, amplitudes and phases can be chosen to perform 0ND, 1ND, 2ND, 3ND or 4ND excitations as fixed waves or backward / forward traveling waves in the rotating frame, in order to mimic, for example, what stator excitation could be like in a truly flow-excited structure. Note that this mechanism allows both synchronous and asynchronous excitations. In the experiments described below on the blisk with the split-ring system, only 2ND, 3ND and 4ND forward traveling waves will be used. Both pseudo-random and stepped sine excitation can be parametrized to obtain frequency response functions (FRFs), depending on whether linear or non-linear behavior is investigated. More precisely, pseudo-random excitation uses synthetic random signal with a spectrum adressing all the frequencies in a range of interest. This is quite quick compared to pure sine excitation but relevant only in linear cases (or when a raw estimate of non-linear peaks location is needed, as a pre-study of non-linearity). Frequency resolution depends classically on the duration of time samples. When non-linearity is expected, stepped-sine is used, with a frequency step equal to the needed resolution: this is much longer considering the time required for each frequency point to be converged on forced response when damping is low. Moreover different levels of excitation are explored. In both cases - pseudo randow and stepped-sine - excitation signal is expanded circumferentially to obtain travelling waves ND patterns.

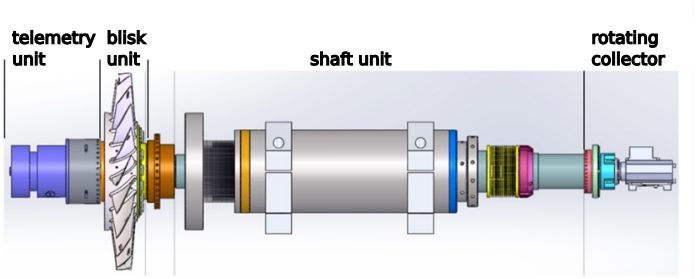

FIGURE 7: CAD VIEW OF THE SPINDLE.

In the configuration used here, the power for each piezoelectric actuator is transmitted from the fixed frame via the hollow shaft through a rotating collector. A study of the target modes' excitability has been done to be sure that significant levels of vibration will be reached, based on the ratio between the strain maps in the piezoelectric actuators area and the amplitudes of blade deflection in the target modes, and also on the calculation of the associated piezo-mechanical coupling factors [22].

2.4 Measurements

The dynamic response of the blisk is measured through 16 metallic strain gauges located at the root of the blades and glued onto the suction side. The number of strain gauges is limited (16 out of 21 blades) due to the telemetry limitation. The location and orientation of the gauges are chosen to maximize the signals to be observed when the modes specific to the first and second families undergo excitation. Their small size makes them well suited to the avoidance of significant perturbations to the test piece. In the early stages of commissioning, crossed calibration of the gauges is performed in the

fixed frame through laser vibrometer measurements, the purpose being to check that the two means of measurement are consistent.

A telemetry system with 16 channels enables signal conditioning, with anti-aliasing filtering, and enables AD conversion to be performed as close as possible to the sensors to minimize signal noise. Special care is then taken at the level of the wiring path to separate high-voltage excitation signals and measurement signals before their treatment by telemetry. Digital signals are then simultaneously sampled and multiplexed and sent to the receiver in the lab's fixed frame through an inductive device mounted at the rear of the blisk.

Piezoelectric drivers provide also low-voltage "images" of the excitation to serve as reference signals for FRFs measurements (conventionally, one piezo is chosen as the reference). Other classical sensors - such as accelerometers, temperature and pressure sensors, tachometer - are used to monitor the rig.

3. SELECTION OF MISTUNING PATTERN

3.1 Use of an AMM ROM model

In this section the selection process for the intentional mistuning is described. For the design of the mistuning pattern, an asymptotic Reduced Order Model (ROM) based on the Asymptotic Mistuning Method (AMM) [17] is used. This is a simple model that only retains a single equation per circumferential harmonic (each equation corresponds to the amplitude of one mass normalized mode of the first modal family). Considering that the blisk is made of N sectors and assuming that the system response is linear, the ROM is expressed as:

$$\left((1+i\beta)\begin{bmatrix}\omega_1^2 & & \\ & \ddots & \\ & & \omega_N^2\end{bmatrix} - \omega_f^2(I+\Delta)\right)\begin{Bmatrix}a_1\\ \vdots\\ a_N\end{Bmatrix} = \begin{Bmatrix}f_1\\ \vdots\\ f_N\end{Bmatrix},$$

where β is the material damping (equal for all the modes), ω_j^2 corresponds to the squares of natural frequencies of the system, ω_f^2 stands for the square of the forcing frequency, a_j represents the complex amplitude of the tuned TW (travelling wave) modes, f_j is the forcing contribution on each TW mode, and Δ is the mistuning matrix. Note that when the system is tuned $\Delta = 0$, all the matrices are diagonal and there is no coupling between TW modes. Therefore, the system is reduced to N scalar equations.

In the general case, however, Δ is a full circulant matrix which couples the different TW modes. The structure of the mistuning is more easily analyzed by looking at the Fourier coefficients of the mistuning pattern [17]. In particular, the Fourier component r of the mistuning pattern couples the TW_j (TW of jth mode) with the TW_{j+r} and TW_{j-r}.

Before using the ROM model, some parameters need to be determined. First, for material damping, a value of $\beta = 9 \cdot 10^{-5}$ was selected, as reported for the same blisk in a previous FUTURE project [19]. The tuned frequencies of the first family were computed with the FEM model in Fig. 1 under a rotation speed of 2000 rpm (see Fig. 8). Only the modes with low ND (ND-1, ND0, and ND1) seem to be affected by the presence of the shaft and hub, and this does not affect the study as the targeted modes have higher NDs.

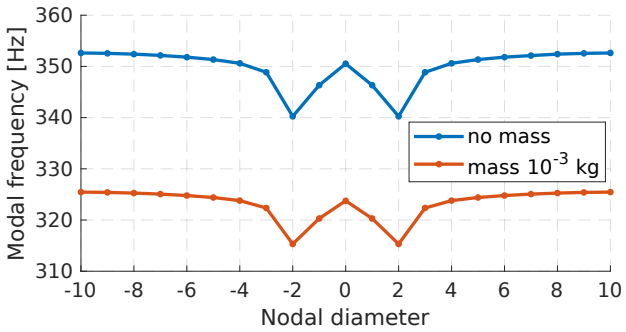

FIGURE 8: NATURAL FREQUENCIES OF TUNED SYSTEM, FROM FEM SIMULATION, ORIGINAL SYSTEM VS SYSTEM WITH 1 G AT EACH BLADE TIP.

To correlate the normalized model on a TW basis, and the FEM model on a physical basis, a second modal analysis is performed including a punctual mass of 1 g on the top of each blade (see the new frequencies in Fig. 8). For this new configuration, the ROM takes the form:

$$\left((1+i\beta)\begin{bmatrix}\omega_1^2 & & \\ & \ddots & \\ & & \omega_N^2\end{bmatrix} - \omega_f^2(1+\delta m)I\right)\begin{Bmatrix}a_1\\ \vdots\\ a_N\end{Bmatrix} = \begin{Bmatrix}0\\ \vdots\\ 0\end{Bmatrix}.$$

Looking at the TW_{10}, the following is obtained:

$$\delta m = \frac{\omega_{10}^2 - \omega_{10,1gr}^2}{\omega_{10,1gr}^2} = 0.148.$$

The interest of studying the combined effect of the split-ring damper and intentional mistuning is to see whether the coupling between TW modes produced by the second is able to activate the ring at modes different from the design mode, here ND2.

3.2 Description of the retained intentional mistuning pattern

Based on this, a specific mistuning pattern denoted [012] was selected. With this pattern, the disk can be regarded as a tuned rotor made of 7 sectors, each of them including 3 blades. The first blade out of the three corresponds to a tuned blade, blade [0]. The second, with a small mass of a certain weight glued at the tip, is blade [1]. And the third blade, with a bigger mass with double weight glued at the tip, is blade [2] (see Fig. 9a).

This [012] pattern is only made up of 3 Fourier coefficients (0, N/3, and 2N/3), as shown in Fig. 9b. These coefficients couple the original tuned TWs in packages of

3 (each TW_j is coupled with the $TW_{j+N/3}$ and $TW_{j-N/3}$), enabling a study of the interaction of the modes in a controlled manner, in contrast to the general mistuned case where all the TWs are coupled. Note that moving 2N/3 in the nodal diameter is equivalent to moving -N/3.

The natural frequencies of the mistuned system are computed with the AMM model, for a value of the small mistuning mass [1] of 0.4 g. The values are plotted in Fig. 10, considering a tuned rotor with 7 sectors. As expected, the introduction of the mistuning masses splits the original modal family into 3 families; the first family dominated by the displacement of the tuned blades [0], the second family dominated by the displacement of the mistuned blades [1], and the third family dominated by the displacement of the mistuned blades [2].

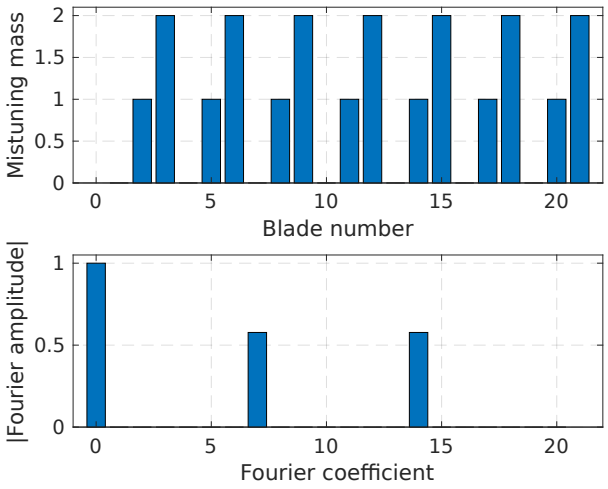

FIGURE 9: (TOP) INTENTIONAL MISTUNING PATTERN [012]. (BOTTOM) FOURIER COMPONENT OF MISTUNING [012].

The selection of the size of the mistuning masses is a compromise between the coupling produced by the mistuning (increasing with the mistuning "size") and safety considerations (the risk of losing one mass under rotation and vibration, and damaging the rig or the blisk, increases with the size of the masses).

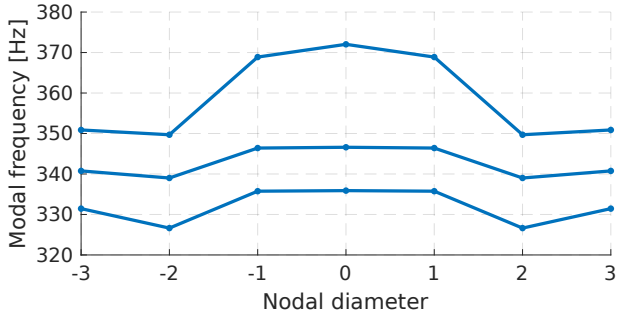

FIGURE 10: NATURAL FREQUENCIES OF AN INTENTIONALLY MISTUNED SYSTEM WITH A SMALL MASS [1] OF 0.4 G.

3.3 Experimental tests on the retuned and mistuned blisk without split-ring

In order to compare the solutions of both systems, and the effect of the mistuning masses, the system was tested before (tuned system) and after the intentional mistuning masses were placed. For these tests, an engine order 2 (EO2) forward traveling wave was used together with a pseudo-random-like excitation. The results for the tuned system are presented at the top of Fig. 11, where the resonances of the excited ND2 and the ND-2 are placed at approximately 337 Hz (the modal analysis overestimation of the frequency is probably caused by the retuning masses added to the real blisk). The resonances of the other NDs are decoupled in first order and the values of the displacement are much lower.

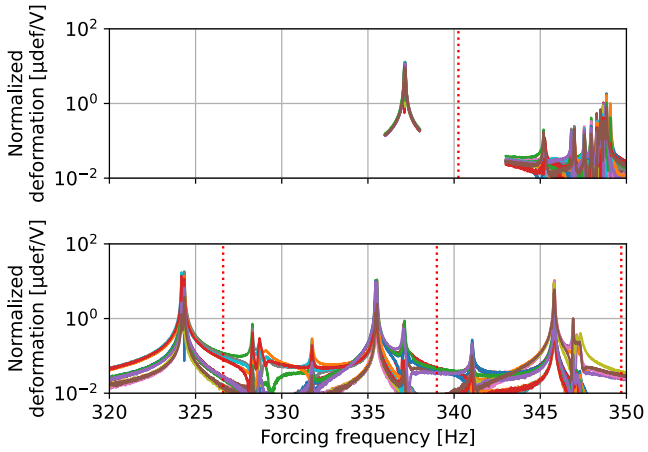

FIGURE 11: EXPERIMENTAL FRFS USING EO2 EXCITATION AND NUMERICAL FREQUENCIES (RED DOTTED LINES): (TOP) TUNED SYSTEM AND (BOTTOM) MISTUNED SYSTEM.

When the same EO2 pseudo-random excitation is applied to the mistuned system, the response shows 3 separate resonances with approximately 10 Hz between each of them (at 324 Hz, 336 Hz and 347 Hz). Each of these resonances has 2 much closer peaks, corresponding to the forward and backward modes, coupled by the natural mistuning. The rest of the resonances have a much smaller amplitude and are not coupled at first order. The experimental response is shown at the bottom of Fig. 11, together with the predicted frequencies. Apart from the drift in frequency, present in the tuned case, the mistuned frequencies are correctly estimated by the model.

The objective of the tests is to see whether this ND2 contribution is sufficient to activate the ring in all 3 resonances.

4. EXPERIMENTAL RESULTS

4.1 Protocol calibration and preliminary results

Before performing the actual tests, the experiment parameters need to be calibrated. The tuned configuration,

rotating at 1500 rpm with the split-ring but without intentional mistuning, is used for this. Some difficulties were encountered due to the blisk characteristics, listed below.

1. Because the nonlinear behavior of the system is sought, a single frequency at a constant tension level has to be excited each time. A stepped sine forcing was used to get the frequency response functions (FRF), instead of faster pseudo-random excitation (used classically for linear systems, and here only to get a rough idea of the location of the FRF peaks).

2. The material damping of the system is very low and the time required to get sufficiently close to the steady state is very high.

3. In relation to the previous point, the frequency "size" of the peaks is very narrow and a very fine resolution in frequency is required to correctly identify damping values.

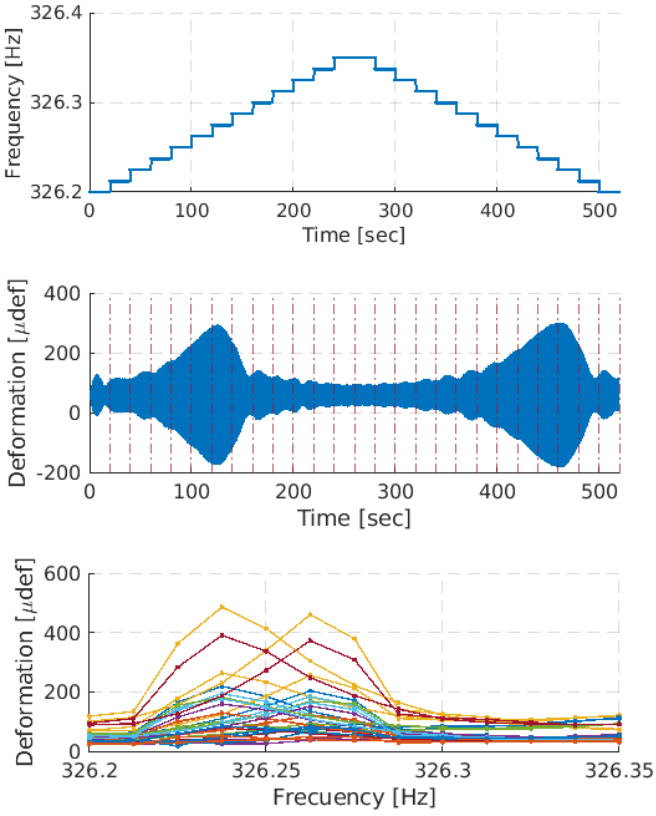

FIGURE 12: SOLUTION OF THE STEPPED-SINE TEST PERFORMED WITH $\Delta\omega$ = 0.0125 HZ AND Δt = 20 S PER ω. (TOP) EXCITATION PATTERN WITH TIME. (MIDDLE) TIME AMPLITUDE OF BLADE 1 DEFORMATION AT ROOT. (BOTTOM) FRF OF ALL BLADES ON 326.20 TO 326.35 HZ FREQUENCY RANGE.

These constraints suggest that the experiments should be performed with a long duration on each frequency and very fine sampling resolution, but only in a narrow range of frequencies so as not to be prohibitively long. Different attempts were made with different size-of-frequency steps (from $\Delta\omega = 0.001$ Hz to $\Delta\omega = 0.025$ Hz), different durations at each step (from 6 s up to 80 s per frequency), and different bandwidths (from 0.1 Hz to 0.3 Hz). An example is shown in Fig. 12, where a single resonance is crossed twice by increasing and then decreasing the forcing frequency. At the bottom, the FRFs are obtained for the 16 probes, and the deformation shown corresponds to the time signal of the reference blade. The comparison with the next set of parameters will show that, with these parameters, the resolution of the resonance curve is not sufficient, and a sufficient approximation of the steady state is not achieved at each frequency.

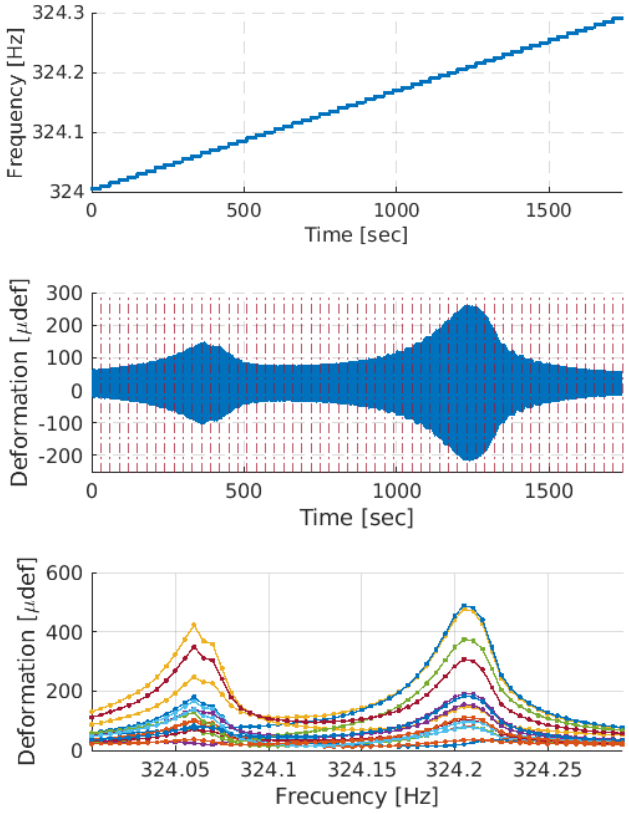

FIGURE 13: SOLUTION OF THE STEPPED-SINE TEST PERFORMED WITH $\Delta\omega$ = 0.005 HZ AND Δt = 30 S PER ω. (TOP) EXCITATION PATTERN WITH TIME. (MIDDLE) TIME AMPLITUDE OF BLADE 1 DEFORMATION AT ROOT. (BOTTOM) FRF OF ALL BLADES IN A 324.00 TO 324.30 HZ FREQUENCY RANGE.

The steady state was qualitatively reached only by testing 80 s per frequency, but the time required for the analysis was too great and a compromise was made. Fi-

nally, the tests were performed with $\Delta\omega = 0.005$ Hz and $\Delta t/\omega = 30$ s, and the frequency was only swept in one direction, with a quite satisfactory agreement with the reference converged test. An example of the results obtained is shown in Fig. 13, where a good resolution of the resonance is obtained (sufficient for damping quantification without significant bias).

However, when performing these tests, an unexpected drift of the resonances with time was found. This drift was associated with an increase in temperature of the blisk caused by the quite high temperature of the telemetry (around $50°C$, heat probably transmitted by conduction). After measuring the temperature of the system, the change in frequency was correlated with titanium softening with temperature (considering a Young modulus change with a temperature of -0.071 GPa/K). This drift made it difficult to correctly capture the resonance curves without performing very long tests. As an example, this drift can be appreciated in the FRF in Fig. 12, where the maximum of the response moved about 0.025 Hz during the 500 s of the test.

The procedure followed in the test campaign consisted in performing a linear test with a pseudo-random excitation before each stepped sine test to capture the resonance locations. The excitation bandwidth of this test was about 2 Hz, which was wide enough to be sure to capture the peaks but small enough to be able to perform fast tests (typically 100 s). After the linear estimation of the location, the test with the incremented-sine forcing was carried out in a narrow region around the resonance peak.

4.2 Seeking the parameters of non-linear behavior activation

Context The split-ring damper is a very complex system, the correct operation of which depends on multiple factors. In this work, at the beginning of the experiments there were still significant uncertainties, mainly with respect to the real friction coefficient in the ring-blisk interface, the prestress level of the ring related to geometric discrepancies in the torus, and the capacity to excite at a sufficient amplitude but without reaching the blisk fatigue limit. Because of this, different tests were performed under different conditions.

The initial purpose was to check the split-ring effect at its design speed under vacuum. But the ring did not behave as expected: no clear activation of the non-linear effect was detected. The campaign objective was thus reoriented to look at maximizing the friction activation under conditions - to be identified - other than those of the design.

With the aim of seeking favorable conditions for activation, different shaft speeds were investigated to release the pressure on the ring-groove interface, the friction coefficient was changed by lubricating the ring, the system was operated at atmospheric pressure to increase the linear damping and to increase the excitation level, and finally the system was forced with different engine orders. These steps are detailed below.

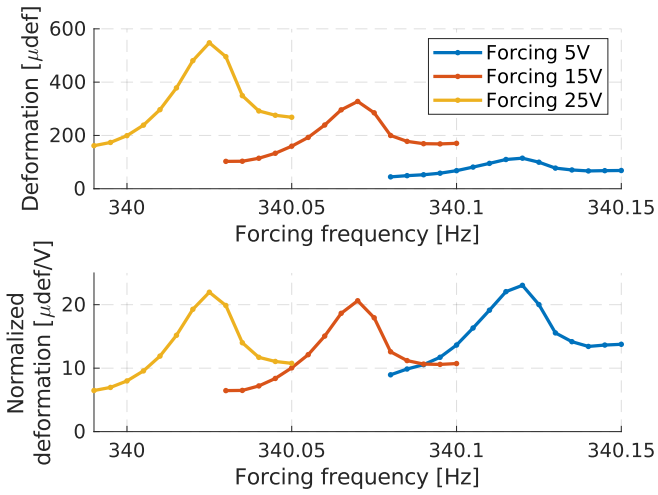

FIGURE 14: MAXIMUM DEFORMATION OF ALL BLADES AT 1700 RPM WITH EO2 FORCING AND SPLIT-RING DAMPER IN VACUUM. (TOP) MODULUS OF FORCED RESPONSE. (BOTTOM) NORMALIZED FRFS.

1. Investigations concerning the rotation speed The initial tests were performed at 4 different rotation speeds: 1700, 1000, 500, and 0 rpm. Starting from the nominal shaft speed, 1700 rpm, the level of normal force in the contact was decreased until only the prestress caused by the spring-back effect of the ring was retained.

The amplitudes obtained with a speed of 1700 rpm and exciting with a forward traveling wave with EO2 are shown at the top of Fig. 14, where a single resonance peak is excited. The results range from a case with low forcing to a case where the stress produced on the blades are close to the fatigue limit. The amplitude of the response grows linearly with the forcing, meaning that there is no activation of the ring. This is more clearly seen at the bottom of Fig. 14, where the resonance curve is normalized with the forcing. As mentioned above, there is a drift of the peaks with time and only relative amplifications must be considered for non-linear behavior assessment.

The results obtained at 1000 rpm and 500 rpm show a similar behavior, without a clear activation of the split-ring friction. It is not until the system is excited at rest that the ring is capable of clearly increasing the damping of the system. The relative resonance curves obtained for different forcing amplitudes and 0 rpm are shown in Fig. 15; the maximum value decreases and the width of the curve increases with the forcing. The ND2 and ND-2 resonances are captured in the results. It is clear that the effectiveness of the ring is higher in the second resonance; this is attributed to the tests being performed at rest and the lack of uniformity of the contact surfaces along the whole ring.

2. Investigations concerning ambient pressure In order to achieve a higher activation of the ring, some tests are performed with the blisk in air. These tests can be performed safely because the rig is not rotating, based on the

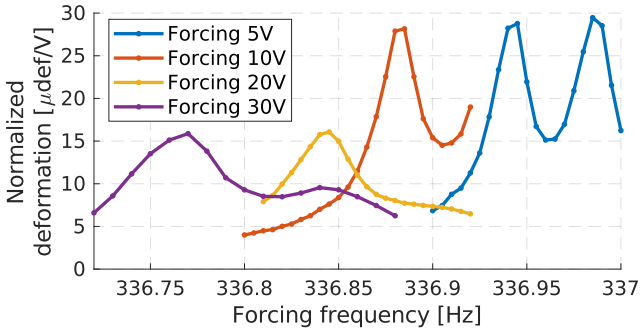

FIGURE 15: NORMALIZED MAXIMUM DEFORMATION OF ALL BLADES AT 0 RPM AND WITH EO2 FORCING OF VARIABLE AMPLITUDE AND SPLIT-RING DAMPER.

previous point. The idea behind this is that, because the blisk's material damping is so small, experiments had to be stopped because the maximum allowed displacement of the blade was reached. Without the vacuum, the damping introduced by air is supposed to allow for a higher excitation force which may activate the split-ring.

The friction at the ring is clearly activated (starting with an excitation of 10 V). The normalized deformations are shown in Fig. 16, where the obtained amplitudes decreased with respect to the tests in vacuum and the maximum allowable damping increased. The growth in damping is sufficient to merge the original 2 peaks for the higher values. This is also seen in Fig. 17 where the normalized deformations of the 16 probes are shown for the case with the highest forcing amplitude.

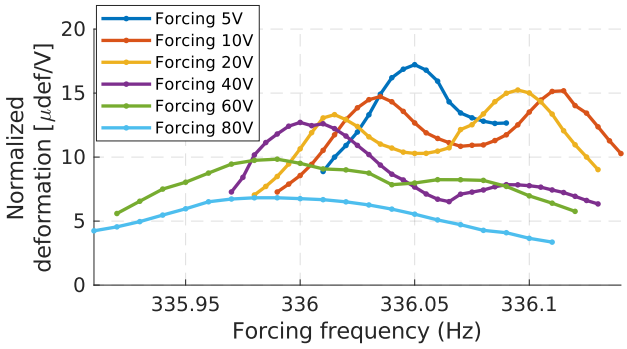

FIGURE 16: NORMALIZED MAXIMUM DEFORMATION OF ALL BLADES AT 0 RPM WITH EO2 FORCING AND SPLIT-RING DAMPER IN AIR.

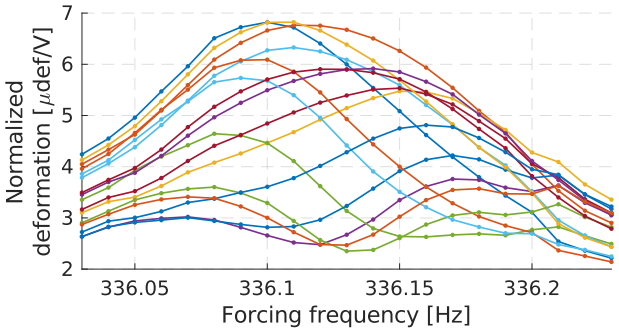

FIGURE 17: NORMALIZED DEFORMATION OF ALL BLADES AT 0 RPM WITH EO2 FORCING AT 80 V AND SPLIT-RING DAMPER IN AIR.

With this configuration, not only the design EO2 forcing, but also the EO3 and EO4 excitations are presented in Fig. 18 (lower levels of excitation are not shown because the response was small and the curves were too noisy).

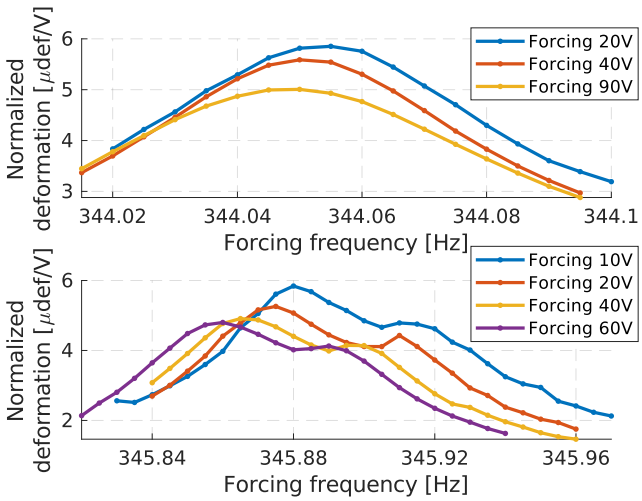

FIGURE 18: NORMALIZED MAXIMUM DEFORMATION OF ALL BLADES AT 0 RPM WITH VARIABLE FORCING AND SPLIT-RING DAMPER IN AIR. (TOP) EO3. (BOTTOM) EO4.

As expected, the highest efficiency of the ring is found for the ND2 mode, with much lower activation in the ND3 and ND4 modes. On EO2 a -58% decrease is observed. On EO3 the normalized deformation amplitude starts to decrease for the highest values of the forcing but with a very low decay. For the case of the EO4 excitation the behaviour is even more quasi-linear (around - 15%).

3. Investigations concerning lubrication The other method investigated to facilitate the activation of the ring, other than running the tests in air, was to lubricate the ring with the objective of reducing the friction coefficient and gaining more sensitivity to the forcing level. The relative resonance curves are presented in Fig. 19. The results are not significantly different from the ones without lubri-

cation. However, the benefits were, first, that the experimental curves obtained were smoother and, second, that the response of the 2 resonant peaks was more homogeneous (smaller difference between peaks).

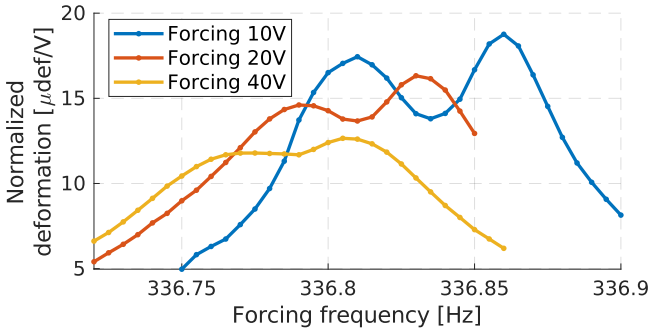

FIGURE 19: NORMALIZED MAXIMUM DEFORMATION OF ALL BLADES AT 0 RPM WITH EO2 FORCING AND SPLIT-RING DAMPER LUBRICATED IN VACUUM.

4.3 Experimental tests on the tuned configuration

To perform the final tests, the two previous strategies are combined; the tests are performed in air and with a ring lubricated only for the non-rotating case. The results are presented in Fig. 20.

For this case, the peaks seemed to merge at an EO2 forcing value smaller than that without lubrication.

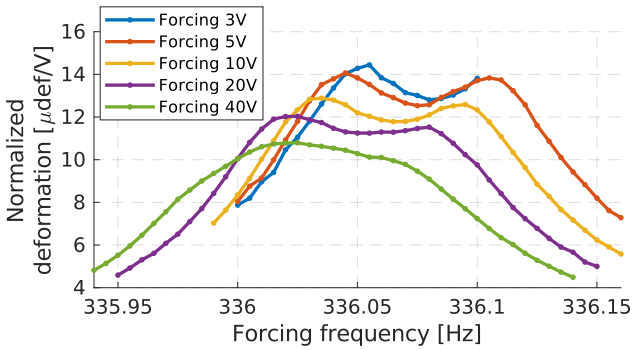

FIGURE 20: NORMALIZED MAXIMUM DEFORMATION OF ALL BLADES WITH VARIABLE EO2 FORCING AND SPLIT-RING DAMPER IN AIR WITH THE RING LUBRICATED.

Finally, the damping ratio was computed using the half-power law to see how it changed with the forcing amplitude (when peaks are too close to clearly identify the -3dB band, an assumption was made to "symmetrize", with respect to peak's frequency, the normalized deformation mode's curve). The results are shown in Fig. 21. Both the values obtained in air with and those obtained without lubrication are shown. The ring is more easily activated with the lubrication, and the damping obtained is higher for the same forcing values.

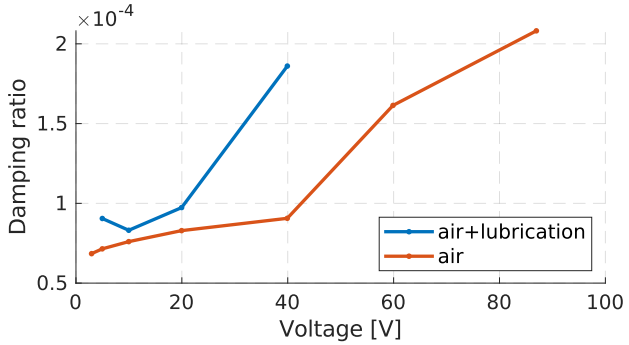

FIGURE 21: EVOLUTION OF DAMPING WITH AMPLITUDE FOR THE DIFFERENT CONFIGURATIONS AT 0 RPM AND EO2 FORCING.

4.4 Experimental tests on the intentionally mistuned configuration with split-ring

Finally, the combined effect of the intentional mistuning and the split-ring was addressed. To do this, the mistuning masses were stuck again for the final experiments. The tests shown were performed with the protocol described above (no rotation, air pressure, and lubrication).

With an EO2 excitation, the system responds in 3 resonances, as described in section 3 and shown in Fig. 11. The 3 resonances were tested with a stepped-sine excitation and the normalized FRFs are shown in Fig. 22. The results show that there is actually an activation of the ring in the 3 resonances. The highest activation occurs in the first resonance and decreases in the second and third ones.

Finally, the evolution of the damping coefficients of the 3 resonances with the forcing amplitude is shown in Fig. 23. Here we can see how the damping increases faster for the first peak than for the second. The values of the damping of the third resonance curve are more constant, meaning that the friction effect is very low, and their values are higher because the forward and backward modes are so close in this resonance that the peaks have merged, giving rise to a wider resonance. However, the damping coefficients are smaller than those obtained in the tuned test for all the peaks.

In Fig. 22, the normalized deformation for variable forcing levels is shown for the excitation of the 3 peaks. It can be seen that the intentional mistuning is actually capable of activating the split ring in different modes, which is precisely the hypothesis under investigation. It can also be seen that the ring is more efficient in the first resonance, in line with the mode content of the solution in each peak - because the tuned TW2 mode is more present in the first resonance than in the others. Based on this, the effect should tend to equalize with the increase in mistuning size. The second conclusion is that although the ring is activated in multiple peaks, its effect is smaller in all of them than that observed in the tuned case (see Fig. 21), and this may not change with the mistuning increment.

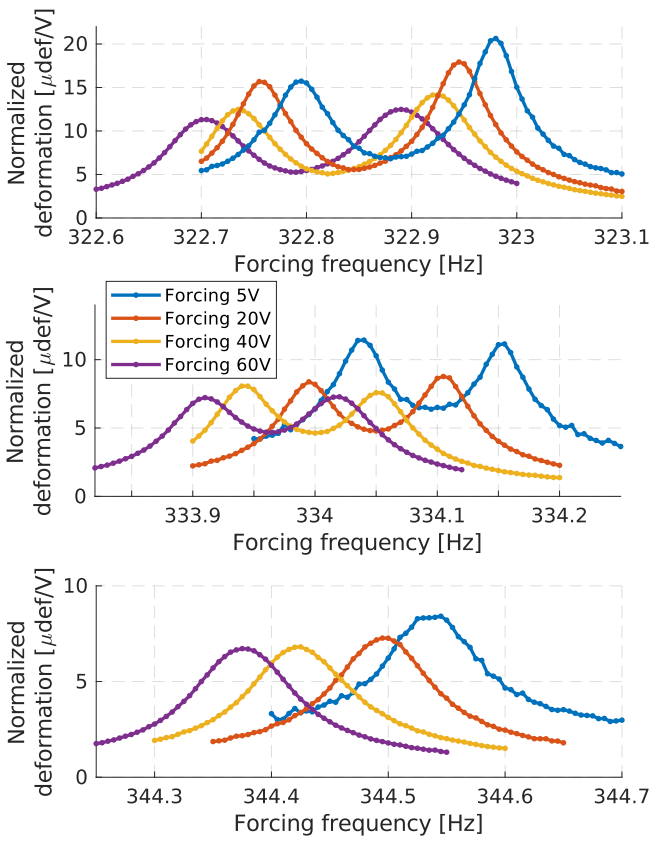

FIGURE 22: NORMALIZED MAXIMUM DEFORMATION OF ALL BLADES AT 0 RPM EO2 FORCING AND SPLIT-RING + MISTUNING IN AIR WITH THE RING LUBRICATED. (TOP) FIRST RESONANCE. (MIDDLE) SECOND RESONANCE. (BOTTOM) THIRD RESONANCE.

5. CONCLUSION

The intentional mistuning pattern chosen has proven to lead to the expected changes in the tuned blisk's modal distribution: it splits the modes into easily identifiable families and couples their responses to traveling wave excitations. Moreover, the experiments confirm the AMM simulations about mistuning implementation.

Concerning the split-ring's non-linear effect, this is found in a narrower region than expected in the design, for both the tuned and mistuned configurations. Operating at rest, lubricating the split-ring, and performing the tests in air gave a clearer view of the activation of non-linearity. In these conditions, the split-ring was activated and showed an increase in the damping from about $5 \cdot 10^{-5}$ to more than $2 \cdot 10^{-4}$ with an EO2 excitation (while there was no clear increment on the damping with EO3 and EO4).

The intentional mistuning pattern induced dissipation in a different mode to the one targeted in the design, in particular in the modes coupled with the ND2 tuned mode by the mistuning pattern. With pattern [012] used, the ring was activated in 3 resonances, but the damping values obtained were smaller than in the tuned configuration. The effect of the friction seems to be "diluted" between the different modes.

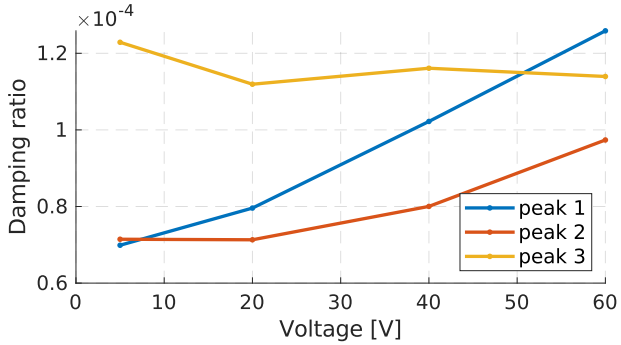

FIGURE 23: EVOLUTION OF DAMPING WITH AMPLITUDE FOR THE DIFFERENT RESONANCE PEAKS.

Forthcoming investigations will be based on these experimental results to revisit non-linear numerical prediction models of forced response with split-ring dampers. They will especially be used to identify potential changes to be made to activate the damper in the real operating design speed: a new design could then be less massive, so that centrifugation does not stick the split-ring in its groove, and so that blade vibration levels can trigger sliding and dissipation without reaching blades' maximum stress limit.

ACKNOWLEDGMENTS

This work has been carried out as part of the ARIAS ("Advanced Research Into Aeromechanical Solutions") project, funded by the European Union's Horizon 2020 research and innovation programme under grant agreement No. 769346 [18].

REFERENCES

[1] Szwedowicz, J., Gibert, C., Sommer, T. and Kellerer, R. "Numerical and Experimental Damping Assessment of a Thin-Walled Friction Damper in the Rotating Set-Up With High Pressure Turbine Blades." *Journal of Engineering for Gas Turbines and Power* Vol. 130 (2008). Doi:10.1115/1.2771240.

[2] Charleux, D., Gibert, C., Thouverez, F. and Dupeux, J. "Numerical and Experimental Study of Friction Damping Blade Attachments of Rotating Bladed Disks." *International Journal of Rotating Machinery* Vol. 2006 (2006). Doi:10.1155/IJRM/2006/71302.

[3] Laxalde, D., Gibert, C. and Thouverez, F. "Experimental and Numerical Investigations of Friction Rings Damping of Blisks." *Proceedings of the ASME Turbo Expo: Power for Land, Sea, and Air, Berlin, Germany*. 2008. Doi:10.1115/GT2008-50862.

[4] Niemotka, M.A. and Ziegert, J.C. "Optimal Design of Split Ring Dampers for Gas Turbine Engines." *Journal of Engineering for Gas Turbines and Power* Vol. 117 (1993): pp. 569–575. Doi:10.1115/1.2814133.

[5] Ye, H., Wang, Y. and Jiang, X. "A Method for the Optimal Design of Split Ring Dampers for Aviation Gears." *Proceedings of the ASME International Design Engineering Technical Conferences and Computers and Information in Engineering Conference, Cleveland, USA*. 2017. Doi:10.1115/DETC2017-67231.

[6] He, X., Zheng, Z., Huang, X., Wang, S., Wei, X., Wang, Y. and Hua, H. "Numerical and Experimental Investigations on a Friction Ring Damper for a Flywheel." *Nonlinear dynamics* (2022)Doi:10.1007/s11071-022-07960-z.

[7] Martel, C., Corral, R. and Llorens, J.M. "Stability Increase of Aerodynamically Unstable Rotors Using Intentional Mistuning." *Journal of Turbomachinery* Vol. 130 No. 1 (2007). Doi:10.1115/1.2720503.

[8] Han, Y., Murthy, R., Mignolet, M.P. and Lentz, J. "Optimization of Intentional Mistuning Patterns for the Mitigation of the Effects of Random Mistuning." *Journal of Engineering for Gas Turbines and Power* Vol. 136 No. 6 (2014). Doi:10.1115/1.4026141.

[9] Tang, W., Baek, S. and Epureanu, B.I. "Reduced-Order Models for Blisks With Small and Large Mistuning and Friction Dampers." *Journal of Engineering for Gas Turbines and Power* Vol. 139 No. 1 (2017). Doi:10.1115/1.4034212.

[10] Laxalde, D., Salles, L., Blanc, L. and Thouverez, F. "Non-linear modal analysis for bladed disks with friction contact interfaces." *Proceedings of the ASME Turbo Expo: Power for Land, Sea, and Air, Berlin, Germany*. 2008. Doi:10.1115/GT2008-50860.

[11] Sun, Y., Yuan, J., Denimal, E. and Salles, L. "A Study of the Contact Interface for Compressor Blisks with Ring Dampers Using Nonlinear Modal Analysis." *Proceedings of the IOP Conference Series: Materials Science and Engineering, Guangzhou, China*. 2020. Doi:10.1088/1757-899X/1081/1/012041.

[12] Wu, Y.G., Li, L., Fan, Y., Zucca, S., Gastaldi, C. and Ma, H.Y. "Design of dry friction and piezoelectric hybrid ring dampers for integrally bladed disks based on complex nonlinear modes." *Computers & Structures* Vol. 233 (2020): p. 106237. Doi:10.1016/j.compstruc.2020.106237.

[13] Mignolet, M., Hu, W. and Jadic, I. "On the Forced Response of Harmonically and Partially Mistuned Bladed Disks. Part I: Harmonic Mistuning." *International Journal of Rotating Machinery* Vol. 6 (2000). Doi:10.1155/S1023621X0000004X.

[14] Willeke, S., Schwerdt, L., Panning, L. and Wallaschek, J. "Intentional Response Reduction by Harmonic Mistuning of Bladed Disks With Aerodynamic Damping." *Journal of Engineering for Gas Turbines and Power* Vol. 140 No. 12 (2018). Doi:10.1115/1.4040898.

[15] Sánchez-Álvarez, J.J. and Martel, C. "Key Action Mechanisms of Intentional Mistuning." *Applied Sciences* Vol. 11 No. 12 (2021). Doi:10.3390/app11125650.

[16] Laxalde, D., Thouverez, F., Sinou, J.J. and Lombard, J.P. "Qualitative Analysis of Forced Response of Blisks With Friction Ring Dampers." *European Journal of Mechanics - A/Solids* Vol. 26 No. 4 (2007): pp. 676–687. Doi:10.1016/j.euromechsol.2006.10.002.

[17] Corral, R. and Martel, C. "Asymptotic description of maximum mistuning amplification of bladed disk forced response." *Journal of Engineering for Gas Turbines and Power* (2009)Doi:10.1115/1.2968868.

[18] The European Commission. "H2020 project 769346, ARIAS: Advanced Research Into Aeromechanical Solutions." (2018-2023)URL http://www.arias-project.eu/.

[19] The European Commission. "FP7 European Project FUTURE: Flutter-Free Turbomachinery Blades." (2008-2012). URL http://www.future-project.eu/.

[20] Pichot, P., Laxalde, D., Sinou, J.J., Thouverez, F. and Lombard, J.P. "Mistuning identification for industrial blisks based on the best achievable eigenvector." *Computers & Structures* Vol. 84 No. 29-30 (2006): pp. 2033–2049. Doi:10.1016/j.compstruc.2006.08.022.

[21] The European Commission. "FP5 European Project ADTurB II: Aeroelastic Design of Turbine Blades." (2000-2004). URL https://cordis.europa.eu/project/id/G4RD-CT-2000-00189.

[22] Ducarne, J. "Modélisation et optimisation de dispositifs non-linéaires d'amortissement de structures par systèmes piézoélectriques commutés." Theses, Conservatoire national des arts et metiers - CNAM. 2009.